Article

Ni/Al$_2$O$_3$/Foam Electric Heating Catalyst: Mitigating Carbon Emissions and Enhancing Reactor Temperature Uniformity

Yanlun Ren [ID], Li Zhang * and Hong Xu *

School of Mechanical and Power Engineering, East China University of Science and Technology,
Shanghai 200237, China; yanlun.ren@ecust.edu.cn
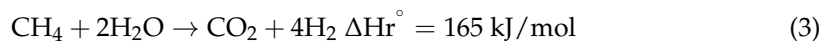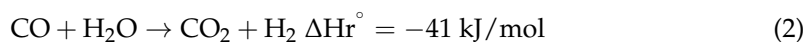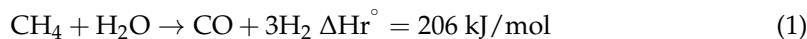* Correspondence: lzhang@ecust.edu.cn (L.Z.); hxu@ecust.edu.cn (H.X.)

Abstract: Substituting the traditional fuel combustion heating mode in hydrogen production reactors with electric heating demonstrates a significant potential for reducing carbon dioxide emissions. An Ni/Al$_2$O$_3$/Ceramic Foam Electric Heating Catalyst was created using a replication template method and a slurry method. On a reactor with dimensions of $\Phi 25 \times 800$ mm, the differences in the heating rate, axial temperature variance, radial temperature variance, and energy consumption between internal and external heating were analyzed. The results show that: (1) By optimizing the structure of the electric heating wires, the temperature uniformity in the catalyst is enhanced; (2) At 650 °C, 3000 h^{-1}, and S/C = 3, compared to traditional granular catalysts, the internal electric heating reduces the axial temperature variance by 69.4% and the radial temperature variance by 95%; and (3) Achieving a temperature of 650 °C using electric heating only requires 23 min, resulting in a 56.82% reduction in energy consumption compared to external heating.

Keywords: steam reforming; foam; joule heating; electrification; decarbonizing

1. Introduction

Achieving energy transformation and reducing carbon emissions are shared global objectives. Hydrogen, an energy carrier and clean alternative to fossil fuels, offers a promising solution, particularly in the petrochemical industry and the production of essential chemicals, like ammonia and methanol [1]. With the expanding global economy, the demand for hydrogen is expected to grow significantly.

Currently, 96% of industrial hydrogen comes from fossil fuels. Out of these, methane steam reforming (MSR) is the most commonly employed and well-established method [2]. The primary reaction processes are outlined below:

$$CH_4 + H_2O \rightarrow CO + 3H_2 \ \Delta Hr^{\circ} = 206 \ kJ/mol \tag{1}$$

$$CO + H_2O \rightarrow CO_2 + H_2 \ \Delta Hr^{\circ} = -41 \ kJ/mol \tag{2}$$

$$CH_4 + 2H_2O \rightarrow CO_2 + 4H_2 \ \Delta Hr^{\circ} = 165 \ kJ/mol \tag{3}$$

Due to the highly endothermic nature of the reaction, the performance of MSR is significantly impacted by the heat and mass transfer characteristics of the production equipment [3]. Insufficient heat supply can lead to sluggish reaction kinetics, while non-uniform temperature distribution within the reactor can cause diminished hydrogen production and catalyst deactivation. Improving temperature distribution has the potential to enhance the performance of MSR [4].

Electrification is regarded as a crucial approach for achieving the decarbonization objective [5]. The industrial MSR reaction occurs in a sizable tubular reactor housing granular catalyst within a robust tube (made of an Ni/Cr alloy, with a thickness of 13–18 mm). A reactor furnace can accommodate 350 10 m-long tubes. The reaction's heat is generated through the combustion of fuel outside the pipeline. This setup encounters challenges

related to limited heat transfer, resulting in low heat transfer efficiency, elevated maintenance expenses, and increased methane fuel consumption [6,7]. It is approximated that the industrial MSR process contributes to approximately 3% of global CO_2 emissions, with fuel combustion accounting for roughly 40% of the CO_2 emissions from the process [8].

Electric heating, in comparison to conventional heating methods, can decrease the temperature difference in the reactor. Its quicker temperature response and higher temperatures offer advantages in terms of thermodynamics, kinetics, and operational constraints. Currently, electric heating methods, such as plasma heating [9], microwave heating [10], and induction heating [11], have been documented. While these heating techniques indeed enhance the reactor's heating rate (°C/min) and reduce carbon emissions, there are some limitations in terms of equipment cost, material requirements, and maintenance costs.

Substituting fossil fuel combustion with Joule heating for energizing the reaction apparatus has emerged as a recent research trend. Currently, Joule electric heating is primarily concentrated in two research avenues: incorporating an electric heater within the device and adopting a structural electric heating reactor. Wismann et al. [12,13] employed a high-resistance tube as a catalyst with a thin layer of nickel coating and utilized electric (Joule) heating to sustain the reforming reaction. This approach is anticipated to potentially reduce carbon dioxide emissions linked to hydrogen production through steam reforming by 20–50%. Rieks [14] applied a thin nickel catalyst coating to silicon carbide in order to enhance heat transfer efficiency, leading to a substantial increase in the heating rate. Currently, despite the significant reduction in heat transfer limitations and increased heating rates achieved by electric heating, there are still issues, such as insufficient catalyst loading, low volume utilization, and limited experience, in pilot-scale applications.

In contrast to conventional tubular or plate heating elements, foam exhibits continuity and pore connectivity, resulting in higher volumetric heat and mass transfer coefficients. This allows for operation at increased space velocities [15]. Selecting open-cell foam as a substrate and applying catalyst coatings are considered the optimal approaches for electrified methane steam reforming (e-MSR) [16].

Badakhs [17] used NiCrAl foam as a carrier for the catalyst, using Joule heating to supply heat for the endothermic ammonia cracking reaction. Dou [18] directly energized the metal foam, which led to rapid heating and a reduced start-up time. However, when applying electric heating to the metal foam catalyst, there is a significant issue of current bypass due to substrate dispersion, necessitating a very high current to reach the desired temperature [19], which restricts its industrial usability.

This research introduces a novel approach to electrically heating methane steam reforming. In this method, electrical energy is directly used to provide heat to the surface of a catalyst foam through resistance heating. The catalyst carrier is made of a corrosion-resistant insulating ceramic, coated with alumina on the surface, and dispersed with a nickel catalyst. This electric heating is evenly distributed within the catalyst. Heat is generated on the surface of the catalyst that requires heating, which enhances the efficiency of heat transfer. Achieving uniform temperatures both vertically and radially is crucial for improving methane conversion efficiency [20].

## 2. Experimental and Simulations

2.1. Methodology

This study introduces an electric heating foam catalyst, which simultaneous fabrication of an electric heating wire and a foam substrate, followed by the deposition of a catalyst coating onto the foam surface. This innovative approach aims to address the challenges associated with high-voltage and -current requirements, difficulties of insulation, and suboptimal coating thickness in conventional electric heating techniques. By doing so, it seeks to optimize the temperature profile within a methane steam reforming reactor, thereby enhancing hydrogen production efficiency, reducing the energy expenditure associated with hydrogen generation, mitigating thermal gradients in the reactor, and bolstering the stability of the catalyst. The thermal characteristics of the electric heating reactor, including

temperature response, axial and radial temperature gradients, and thermal efficiency, were comprehensively assessed using experimental methodologies. Additionally, the impact of the electric heating wire distribution on the internal temperature uniformity of the electric heating catalyst was qualitatively analyzed using numerical simulation techniques. Through the above description, we can divide the Methodology Section into two parts: experiment and simulation.

2.2. Experiment

2.2.1. Ni/Al$_2$O$_3$/Ceramic Foam Preparation

The commercial polyurethane sponge (20 PPI, where PPI represents pores per inch) was processed into a cylindrical shape with a length of 800 mm and a diameter of 25 mm, as shown in Figure 1a. The polyurethane foam was sonicated in a deionized water and acetone solution for 20 min (300 W), and then immersed in a 1 M NaOH solution (50 °C) for 24 h. The soaked polyurethane foam was rinsed in deionized water for 20 min, dried at 70 °C for 1 h, and implanted with an electric heating wire (FeCrAl, wire diameter: 1 mm). Finally, it was placed in a 20% concentration of tetramethylammonium hydroxide solution for 20 min, rinsed in deionized water for 20 min, and dried at 100 °C for 2 h.
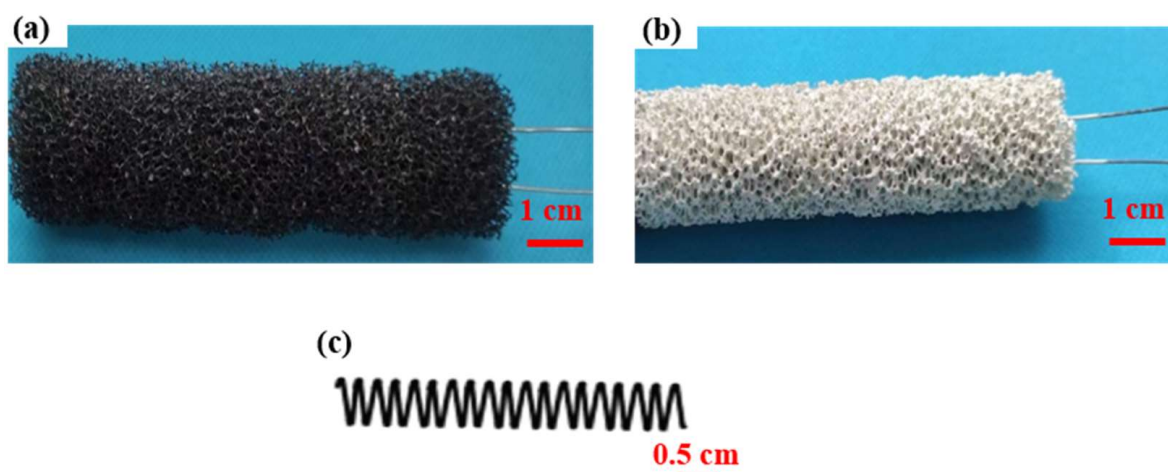
Figure 1. Catalyst preparation diagram: (**a**) foam before calcination; (**b**) foam catalyst after calcination; (**c**) internal electric heating wire.

The slurry was prepared with γ-Al$_2$O$_3$, calcium aluminate, glass fiber, kaolin and aluminum stearate, and milled for 30 min. The treated sponge was immersed in the slurry for 15 min, the excess slurry was blown off, dried at 70 °C for 2 h, heated to 300 °C at a rate of 5 °C/min, calcined for 1 h, and then heated to 1200 °C for 2 h to prepare an electrically heated foam carrier. The prepared electrically heated foam carrier was impregnated with a γ-Al$_2$O$_3$ solution (γ-Al$_2$O$_3$ 20 wt.%), the excess slurry was purged, dried at 120 °C, and then heated at a rate of 5 °C/min to 600 °C for 2 h. Subsequently, the carrier was immersed in a 20 wt. % nickel nitrate solution for 6 h, then dried at 100 °C for 120 min, and calcined at 600 °C for 120 min under the protection of N$_2$ to prepare an electrically heated catalyst. The form of electric heating wire is shown in Figure 1c, and the prepared foam electric heating catalyst is shown in Figure 1b. At a high temperature, the slurry was attached to the original polyurethane skeleton to form a support, replicate the organic foam structure, and the electric heating wire and the foam skeleton were integrated to prepare an in situ electric heating catalyst.

2.2.2. Catalyst Characterization and Catalytic Activity Tests

(1) Catalyst characterization

The surface morphology was examined using a German scanning electron microscope. The electric heating catalyst's electric heating wire was linked to a DC power supply (Dongguan Maisheng Power Supply Technology Co., Ltd., Dongguan, China, MS1520DS). Temperature control was achieved through a solid-state relay (Delixi Electric Co., Ltd., Yueqing, China, CDG1-1DD) and a temperature control instrument (Xiamen Yudian Automation Technology Co., Ltd., Xiamen, China, AI516), while the reactor's temperature was monitored using an Agilent 34,972 A temperature acquisition instrument and k-type thermocouple. The temperature was measured with a Φ1 mm K-type thermocouple (Platinum Sensor Co., Ltd., Petersfield, UK).

External heating involves placing the reactor inside a 2 kW electric heating furnace, and the reactor's temperature was regulated by the furnace program. In contrast, internal electric heating entails connecting the internal electrode of the catalyst to the DC power supply, with the external furnace remaining inactive, and temperature control was managed with a temperature control instrument. Both internal and external heating methods were employed to attain the same temperature, and the reactions were conducted under identical conditions. The power consumed for internal and external heating was calculated using the standard Kang BK-034-16 A power digital-display socket meter manufactured by Shanghai Newhui Industrial Co., Ltd., Shanghai, China, Additionally, a U-tube (Shanghai Kuangjian Instrument Technology Co., Ltd., Shanghai, China) was used for conducting reactor pressure drop tests. The specific parameter information of the catalyst is shown in Table 1.

**Table 1.** Properties of different catalysts.

Sample	Heat Form	Parameter	Catalyst Loading
ES-In	Internal electric heating	Foam catalyst [21], hole spacing: 1 mm, opening rate: 90%, hole number: 400/square inch	43.4 g/180 mL
GC-Out	External electric heating	Granular catalyst, commercial Ni-Al$_2$O$_3$ catalyst [22], particle size: 0.45–0.9 mm	137 g/180 mL
ES-Out	External electric heating	Foam catalyst, hole spacing: 1 mm, opening rate: 90%, hole number: 400/square inch	43.4 g/180 mL

(2) Catalytic activity tests

The catalyst reaction performance evaluation system is illustrated in Figure 2a. The in situ electric heating foam catalyst is enclosed within a thermally conductive liner and placed inside a tubular reactor with a 25 mm inner diameter. To ensure device airtightness, a soap water detection method was employed.

The catalyst underwent reduction at a space velocity of 1000 h^{-1}, with a gas mixture of 10 wt. % H$_2$ and the remaining nitrogen at a temperature of 600 °C for 2 h. Subsequently, the system was purged continuously with nitrogen for 30 min. The actual reaction took place inside the reactor, with temperatures ranging from 600 °C to 800 °C, using a preheating temperature of 400 °C, a reaction volume space velocity of 4000 h^{-1}, and a feed gas ratio of n (H$_2$O)/n (CH$_4$) = 3.0. After 30 min of reaction stabilization, a gas–liquid separation device removed water from the gas stream, which was then analyzed for its gas composition using a gas chromatography analyzer. The feed gas was methane (99.99%, with the remaining being N$_2$) obtained from Shanghai Wei Chuang Standard Gas Co., Ltd., Shanghai, China.
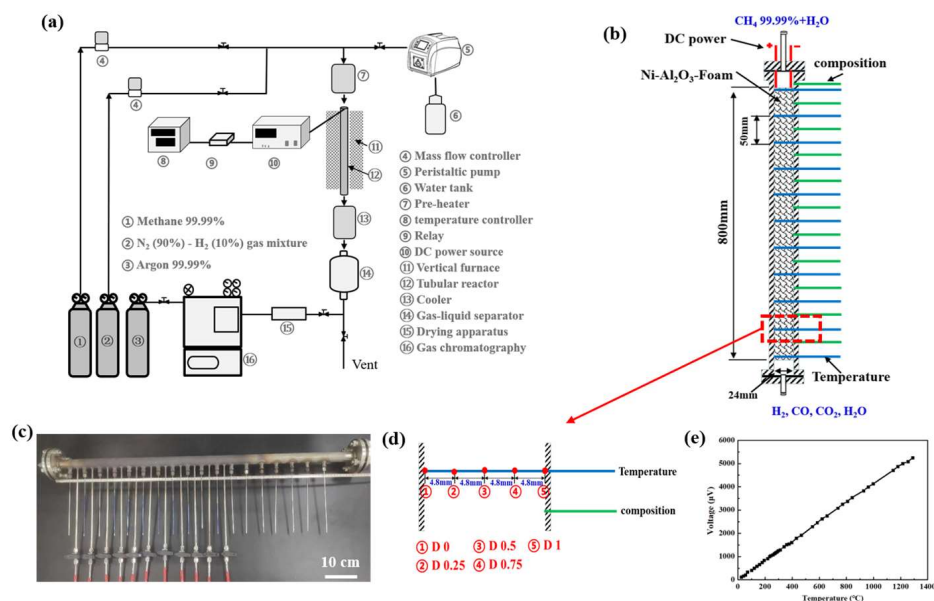
Figure 2. Catalyst performance evaluation device. (**a**) Evaluation device system; (**b**) distribution of reactor test points; (**c**) reactor; (**d**) radial temperature difference test point distribution; (**e**) thermocouple curve.

For monitoring the reaction products at different intervals, measuring holes were introduced at 5 cm intervals along the reactor wall, and the composition was determined using an Agilent 7890A gas chromatograph (GC). Temperature measurements were taken at 5 cm intervals within the reactor by extending thermocouples to the inner wall. The internal reactor temperature was monitored using an Agilent 34972A temperature acquisition instrument, allowing for the analysis of axial and radial temperature variations.

2.2.3. Equations

The methane conversion rate and the selectivity of each gas were determined using the following calculations:

Methane conversion rate:

$$X_{CH_4} = \frac{[F_{CH4}]in - [F_{CH4}]out}{[F_{CH4}]in} \times 100\% \tag{4}$$

Gas selectivity:

$$X_{H2} = \frac{F_{H2}}{[F_{CH4}]in - [F_{CH4}]out} \times 100\% \tag{5}$$

$$X_{CO} = \frac{F_{CO}}{[F_{CH4}]in - [F_{CH4}]out} \times 100\% \tag{6}$$

Hydrogen production per unit mass of catalyst:

$$Q_{m_{H_2}} = \frac{F_{out} \times C_{H_2}}{m} \tag{7}$$

Hydrogen production per unit volume of reactor cavity:

$$Q_{V_{H_2}} = \frac{F_{out} \times C_{H_2}}{V} \tag{8}$$

where $[F_{CH4}]in$ and $[F_{CH4}]out$ are the volume flow rate of methane entering and exiting the reactor, respectively, mL/min. The F_{H2} outlet is the volume flow rate of hydrogen exiting the reactor, mL/min. The F_{CO} outlet is the volume flow rate of carbon monoxide exiting the reactor, mL/min. The F_{out} outlet is the volume flow rate of product gases exiting the

reactor, mL/min. C_{H2} corresponds to the volume fraction of the substance in the product gas [23].

$$
\begin{aligned}
(F_{CH4,in} \times cp_{CH4,in}) \times (T_{CH4,in} - T_{rif}) + (F_{H2O,in} \times cp_{H2O,\,in}) \times (T_{H2O,in} - T_{rif}) - (F_{CH4,out} cp_{CH4,\,out} \\
+ F_{H2O,out} \times cp_{H2O,out} + F_{CO,out} \times cp_{CO,out} + F_{CO2,out} \times cp_{CO2,out}) \times (T_{gas,out} - T_{rif}) - (F_{CH4,in} \\
- F_{CH4,out}) \times \Delta H°_{R.Trif} SR + (F_{CO2,in} - F_{CO2,out}) \times \Delta H°_{R.Trif} WGS + Q_{MJ} - Q_{diss} = 0
\end{aligned}
\tag{9}
$$

where F_i = molar flow rates entering and exiting the reactor; C_p = specific heat.

$T_{gas,\,in}$ = temperature at the inlet, 25 °C; $T_{gas,\,out}$ = temperature at the outlet of the reactor; T_{rif} = reference temperature, 25 °C; $T_{H2O,\,in}$ = temperature of H_2O at the inlet, 200 °C; $\Delta H°_{R.Trif}$ = standard enthalpy at 25 °C; Q_{MJ} = heat supplied by means of joule heating; and Q_{diss} = heat dissipated by the system.

$$
Q_{diss} = \left(\sum T_{i,1} - \sum T_{i,2} \right) / (t_{i1} - t_{i2})
\tag{10}
$$

where T_{i1} = Temperature when heating is stopped, T_{i2} = Temperature when heating is end-stopped, t_{i1} = Time when heating is stopped, and t_{i2} = Time when heating is end-stopped.

2.3. Simulation

The three-dimensional model, constructed utilizing 3D software, was subsequently imported into the finite element analysis platform, COMSOL Multiphysics version 5.4. For the simulation of the reaction gas flow in the network structure catalyst, the 'free and porous media flow' interface was used to calculate the velocity distribution of the reaction gas in the bed. For the simulation of the heat transfer and hydrogen production performance of the bed height with the reaction, it was also necessary to use the 'dilute mass transfer' interface to simulate the component transport process, and the 'porous medium heat transfer' interface to simulate the heat transfer phenomenon with the reaction source phase in the bed. After selecting the interface to be used in the simulation, the corresponding boundary conditions needed to be set.

Following the establishment of boundary conditions and the assignment of fluid physical parameters, the computational domain was discretized into a mesh aligned with the physical field characteristics. A comparative analysis of models with varying grid sizes revealed that the impact of regular grid size on methane conversion could be considered negligible. Subsequently, the finite element method was employed to solve the ensuing equations, with a convergence tolerance of 10^{-3} set for each variable.

The governing equation for fluid motion is the Navier–Stokes equation. For the case of steady, incompressible fluids, the influence of gravitational forces was deemed insignificant. The standard equation definition (heat transfer), continuity equation, momentum conservation equation, component transport equation, and energy equation were defined by referring to the methods in the references [24,25].

2.3.1. Geometric Model

Figure 3 illustrates the geometric structure model. In this study, the simulation was conducted using a tubular reactor with dimensions of Φ25 mm × 800 mm.
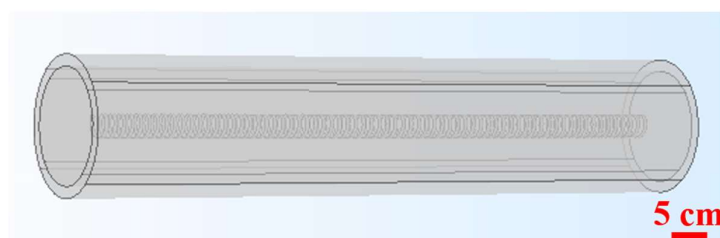

Figure 3. Geometric model.

2.3.2. Nomenclature

The model consists of a reaction tube and an electrically heated catalyst. In order to simulate the electric heating characteristics of FeCrAl matrix, the 'current' interface was added. The electric heating substrate was applied as a resistance to the potential boundary, and the loaded potential difference was controlled by the outlet temperature. The inlet boundary condition is the velocity inlet boundary condition, the outlet boundary condition is the pressure outlet boundary condition, and the outlet pressure is 0. The symmetry surface adopts symmetrical boundary conditions. The ohmic heating heat source of the FeCrAl substrate domain was zero, and the heat source of the other domain was zero. Electric heating is defined according to the Ohm's law, and electric heating is applied to generate heat. The calculation accuracy and convergence criteria were set by default.

In the previous work, the temperature response characteristics of electric heating foam catalyst were verified [21]. In order to further optimize the temperature uniformity of electric heating foam catalyst, five aspects of wire characteristics were studied. The nomenclature of the electric heating wire parameter optimization simulation inside the electric heating foam are shown in Table 2.

Table 2. Electric heating foam catalyst nomenclature.

Sample *	Form	Wire Diameter mm	Pitch mm	Spiral Diameter mm	Number
EL-F-01	linear	0.8	/	/	/
ES-F-02	spiral	0.8	4	5	/
ES-W-01	spiral	1	4	5	/
ES-W-02	spiral	1.2	4	5	/
ES-W-03	spiral	1.5	4	5	/
ES-S-01	spiral	0.8	4	2	/
ES-S-02	spiral	0.8	4	3	/
ES-S-03	spiral	0.8	4	4	/
ES-S-04	spiral	0.8	4	5	/
ES-P-01	spiral	0.8	2	5	/
ES-P-02	spiral	0.8	4	5	/
ES-P-03	spiral	0.8	6	5	/
ES-N-01	spiral	0.8	2	5	2
ES-N-02	spiral	0.8	2	5	3
ES-N-03	spiral	0.8	2	5	4

* Sample codes. L represents linear, the first S represents spiral, F represents form, W represents wire diameter, P represents pitch, the middle S represents spiral diameter, and N represents number.

2.3.3. Boundary Conditions and Parameter Values

The boundary conditions set in this paper are shown in Table 3. The material properties of the reactor and the physical parameters of each fluid component are specified, as shown in Table 4.

Table 3. Setting of boundary conditions.

| Category	Attribute
Boundary	Type of boundary conditions
Reactor inlet	Speed inlet, temperature inlet
reactor outlet	Pressure outlet
External surface of the reactor	Wall (adiabatic)
Inner surface of reactor	Coupling

Table 4. Parameter values used in the calculation model.

Category	Attribute	Value	Units
Foam	density	1500	kg/m^3
	heat capacity at constant voltage	950	J/m^3
	thermal conductivity	5	W/(m·K)
	porosity	85%	1
Heating wire	electric conductivity	106	S/m
	relative dielectric constant	1.2	1
	thermal conductivity	18.3	W/(m·K)
	density	7800	kg/m^3
	heat capacity at constant voltage	500	J/(kg·K)
	specific heat capacity	1.23	1
Stainless steel	thermal conductivity	40	W/(m·K)
	density	7900	kg/m^3
	heat capacity at constant voltage	500	J/(kg·K)
Gas	thermal conductivity	k(T [1/K]) [W/(m.K)]	W/(m·K)
	heat capacity at constant voltage	C(T [1/K]) [J/(kg·K)]	J/(kg·K)
	density	rho_gas_2(T [1/K]) [kg/m^3]	kg/m^3
	specific heat capacity	1.2	1

2.3.4. Model Validation

In this paper, the numerical simulation was affected by the following assumptions: (1) the gas flow was incompressible laminar flow in steady state; (2) the influence of gravity on airflow was neglected; (3) the catalyst layer domain was regarded as a homogeneous and isotropic porous medium; (4) the chemical reaction only occurred in the catalyst layer domain; (5) the effect of heat loss was neglected; (6) the electric heating wire was considered to be pure resistance; and (7) the catalyst coating was non-conductive. Therefore, there will be some errors, so we performed a model validation.

As depicted in Figure 4, it is evident that, under identical experimental and simulation conditions, the simulated curve trajectory closely aligns with the central axis temperature distribution observed in the experiment. The maximum error between the simulated value and the experimental value is less than 6%, and the change trend is basically the same under different reaction temperature. This provides confirmation of the accuracy and reliability of the tubular reactor model.
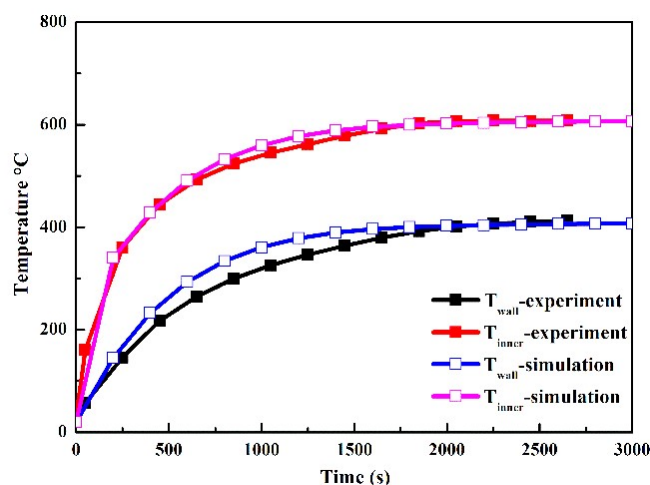
Figure 4. Model validation.

3. Results and Discussion

3.1. Catalytic Performance and Heating Characteristics

A catalyst measuring Φ25 mm $\times$ 800 mm was prepared, as depicted in Figure 5. The figure illustrates the complete bonding of internal particles within the electrically heated foam, integrating the electric heating wire and the foam matrix into a cohesive structure during the molding process. This integration effectively minimizes the thermal resistance between the electric heating wire and the foam matrix, consequently enhancing the catalyst's heat transfer performance. Through the optimization of the electric heating wire distribution within the foam matrix, the overall temperature uniformity of the electrically heated catalyst can be significantly enhanced.
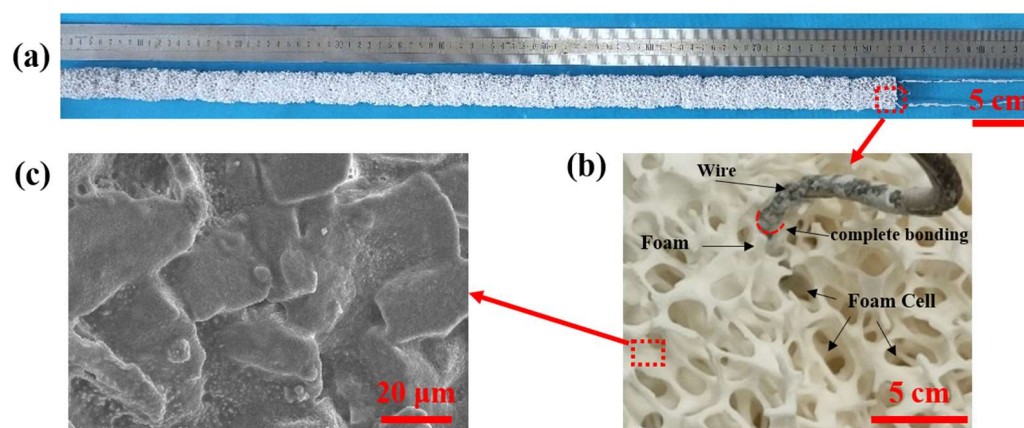

Figure 5. Ni/Al$_2$O$_3$/Ceramic foam electric heating catalyst. (**a**) Foam electric heating catalyst; (**b**) 10.0$\times$; (**c**) 1000.0$\times$.

The experimental results demonstrate that the electrically heated catalyst reaches 650 °C from room temperature in just 23 min. This rapid heating is attributed to the generation of Joule heat by the internal electric heating wire of the catalyst upon energization, swiftly raising the outer foam catalyst to the target temperature. The temperature rise curve is depicted in Figure 6.

From Figure 6a, it is evident that, under constant resistance, the temperature rise rate significantly accelerates with the increase in the power or current, rising from 15 °C/min to 38 °C/min. The temperature rise characteristics based on Joule heating are positively correlated with power. From Figure 6b, it can be observed that this internal-to-external heating form can reduce heat loss. When the temperature inside the reactor is maintained at a constant 650 °C, the highest temperature on the outer wall is 150 °C. The reduction in heat dissipation can effectively enhance the reactor's energy efficiency, improve the electric heating efficiency, and system thermal efficiency.

At the same power, resistance, and external insulation conditions, the temperature curves of the electrically heated catalyst under different gas hourly space velocity are illustrated in Figure 6c. Due to the internal-to-external heat supply and the close proximity between electric heating and foam catalyst, the overall system exhibits excellent temperature response characteristics. This ensures that the internal temperature of the reactor does not undergo significant variations with changes in gas flow rates, resulting in a highly stable temperature profile.
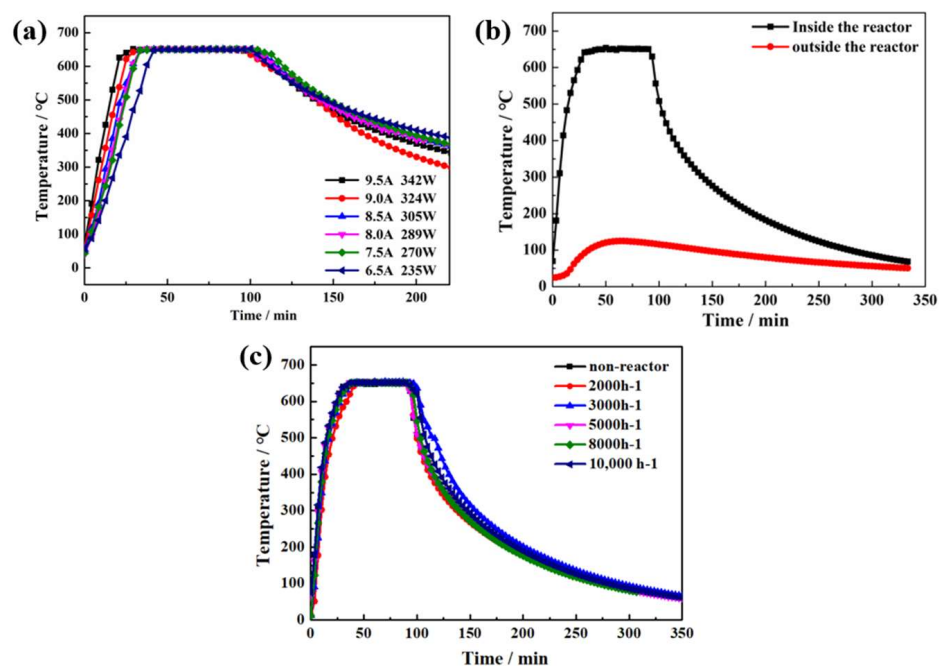
Figure 6. Heating characteristics of electric heating. (**a**) Heating curve at different power; (**b**) Internal and external temperature difference of the reactor at 9.5 A 342 W. (**c**) Temperature rise curves under different gas flow rates.

The heat dissipation power and energy efficiency during the electric heating process are illustrated in Figure 7. It can be observed that, with the increase in temperature, the heat dissipation of the electrically heated catalyst significantly rises, reaching 72% energy efficiency at 650 °C. Further enhancement of the catalyst's energy efficiency can be achieved through external insulation or optimization of electric heating.
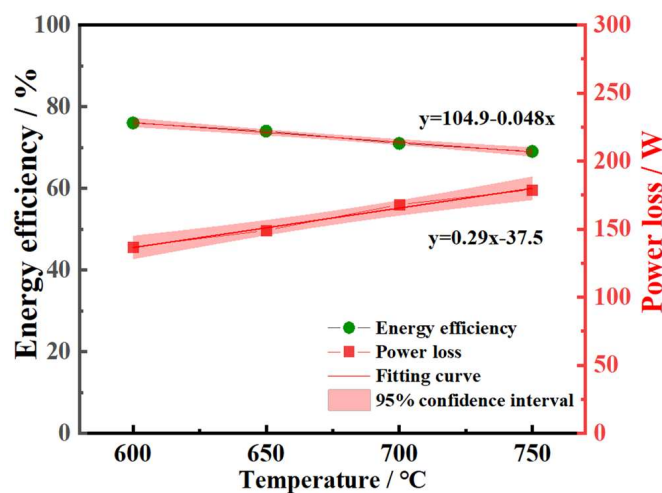
Figure 7. Energy efficiency of electric heating catalyst.

The electric heating wire produces Joule heat, which transfers from the inside to the outside. As a result, the whole reactor is uniformly heated, creating a 'volume heating'effect that reduces the power consumption and increases the heat transfer rate. At 650 °C, S/C = 3, and 3000 h^{-1}, the catalyst's performance is illustrated in Figure 8. Because the reaction temperature is more uniform and there is no heat transfer limitation, the methane content in the product gas is less than 5%, and the methane conversion rate is higher than 90%. The conversion rate of the catalyst remains stable, with no significant changes in hydrogen and carbon monoxide concentrations.
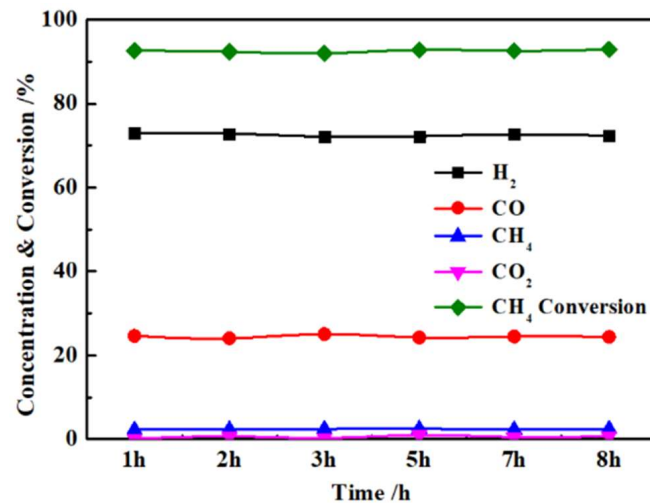
Figure 8. Catalyst performance curve.

3.2. Temperature Distribution of Electric Heating

In order to optimize the distribution of the heating wire within the catalyst and adjust the temperature uniformity inside the electrically heated foam catalyst, structural form, final diameter, spiral diameter, spiral pitch, and the number of spiral wires of the heating wire were optimized. The heating wire material and external foam material were kept consistent, as well as the preparation method. However, the variation in the number of wires and the electrical heating structure leads to deviations in the total length of electrical heating within the catalyst. Therefore, this optimization section aimed to analyze the temperature variation inside the reactor by solely controlling the current at 9A, while disregarding the differences in electrical heating power.

Influence of the form of wire. Figure 9 illustrates the comparison of the impact of the internal wire configuration of the foam electric heating catalyst on temperature distribution. In Figure 9a, it can be observed that the temperature difference between the central temperature and the coldest point at the edge is 335.0 °C for the straight wire configuration. Simultaneously, apart from the wire itself, most other areas exhibit temperatures lower than 400 °C. In contrast, for the spiral wire catalyst, the highest and lowest temperatures in the center are 273.8 °C, which is 18.27% lower than that of the single-strand wire catalyst. This indicates that the temperature distribution within the catalyst is more uniform with the spiral wire configuration. In Figure 9a, the temperature in the majority of the reactor's regions significantly deviates from the desired target of 600 °C, with the exception of the electric heating wire itself, which has reached a temperature of 612 °C. In comparison to ES-F-01, ES-F-02 exhibits a more extensive distribution of the electric heating wire within the catalyst. This increased presence of electric heating wires contributes to a more uniform internal temperature distribution.
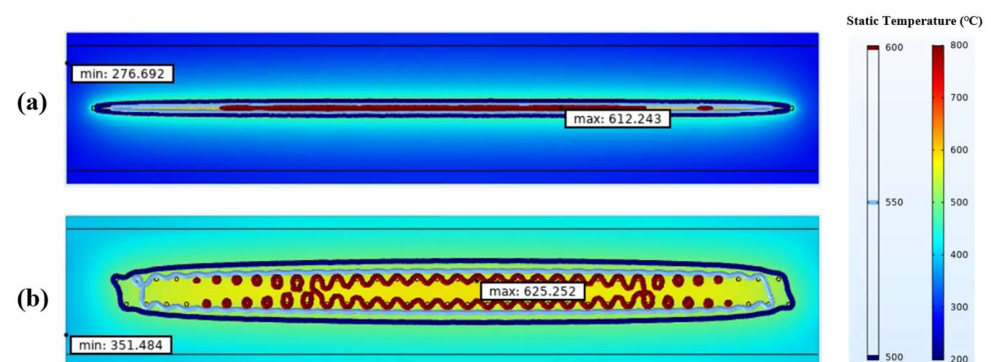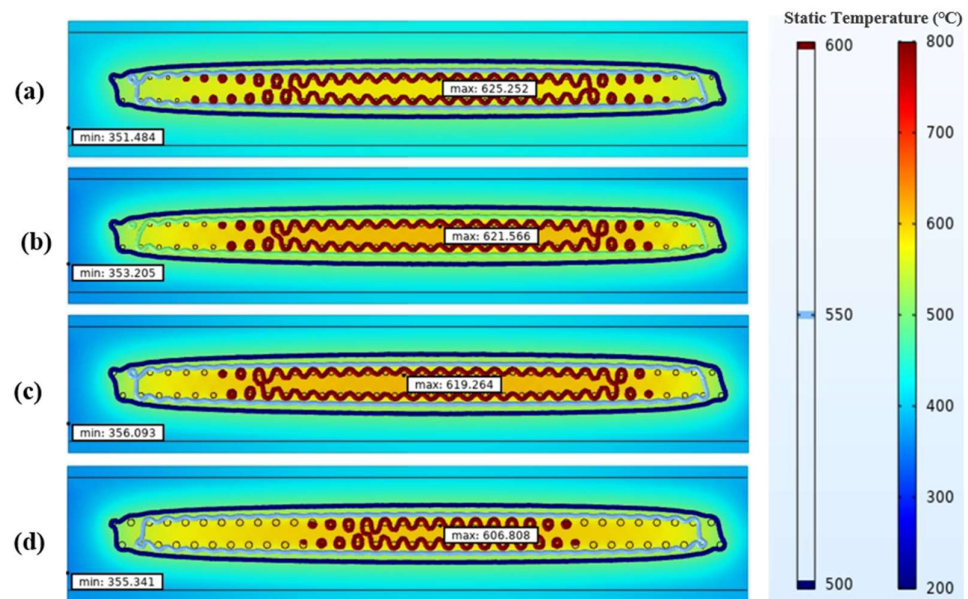

Figure 9. Temperature distribution isotherms: (**a**) ES-F-01 and (**b**) ES-F-02.

Figure 10 presents a comparison of the impact of the diameter of the electric heating wire on temperature distribution. It is evident that as the wire diameter increases, the temperature difference between the highest and lowest points decreases, measuring 273.8 °C, 267.9 °C, 263.2 °C, and 251.5 °C. This temperature decrease is consistent with the increase in wire diameter, showing a positive correlation between them. However, upon closer examination, it becomes apparent that the temperature change in the coldest region is not as pronounced, and the decrease in the temperature difference primarily stems from the reduction in the highest temperature region.

$$R = \frac{\rho \times L}{S} \tag{11}$$

$$Q = I^2 \times R \times t \tag{12}$$

Figure 10. Temperature distribution isotherms: (**a**) ES-F-02, (**b**) ES-W-01, (**c**) ES-W-02, and (**d**) ES-W-03.

In these equations, R represents resistance, ρ denotes resistivity, L signifies the length of the wire, and S stands for the cross-sectional area. Q represents the heat produced due to resistance, I corresponds to the current passing through the resistance, and t represents the heating duration.

The wire's resistance is directly proportional to its resistivity and inversely proportional to its cross-sectional area (S). An increase in the wire diameter results in a larger cross-sectional area, leading to reduced resistance. According to Equations (11) and (12), the heat generated by the resistor is proportional to the square of the current, the resistance of the resistor, and the heating time. When the current and voltage remain constant, lower resistance leads to a decrease in the overall temperature. However, the choice of wire diameter also needs to take into account processing difficulty and strength. A wire diameter of 1 mm was preferred as the final choice.

Figure 11 illustrates the impact of the spiral diameter of the foam electric heating catalyst on temperature distribution. It is evident that, as the spiral diameter of the catalyst increases, the temperature difference between the highest and lowest points decreases, measuring 393.6 °C, 330.1 °C, 305.1 °C, and 273.8 °C. The temperature gradually decreases, and an increase in the spiral diameter is advantageous for reducing the temperature difference. With a larger spiral diameter, the temperature is distributed more evenly throughout the entire foam matrix, resulting in a smaller temperature difference. Considering insulation and preparation challenges for a reactor with a 25 mm inner diameter, a preferred spiral diameter of 5 mm is recommended.
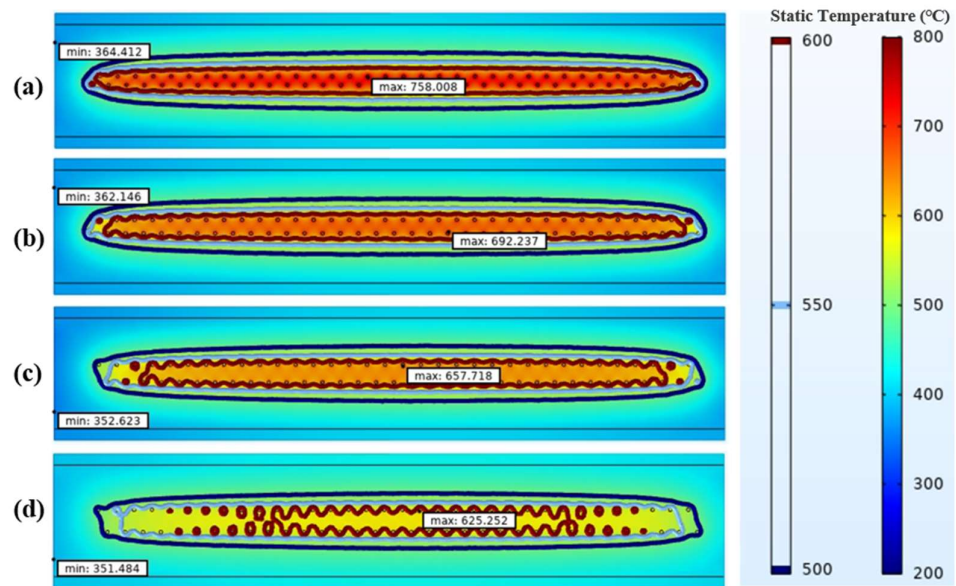
Figure 11. Temperature distribution isotherm diagram: (**a**) ES-S-01, (**b**) ES-S-02, (**c**) ES-S-03, and (**d**) ES-S-04.

Figure 12 provides a comparison of the impact of helical pitch on the temperature distribution of the foam electric heating catalyst. With an increase in pitch, the temperature difference gradually expands, and the demarcation between the high-temperature and low-temperature regions inside the catalyst becomes more apparent. This results in a less uniform temperature distribution throughout the entire catalyst.
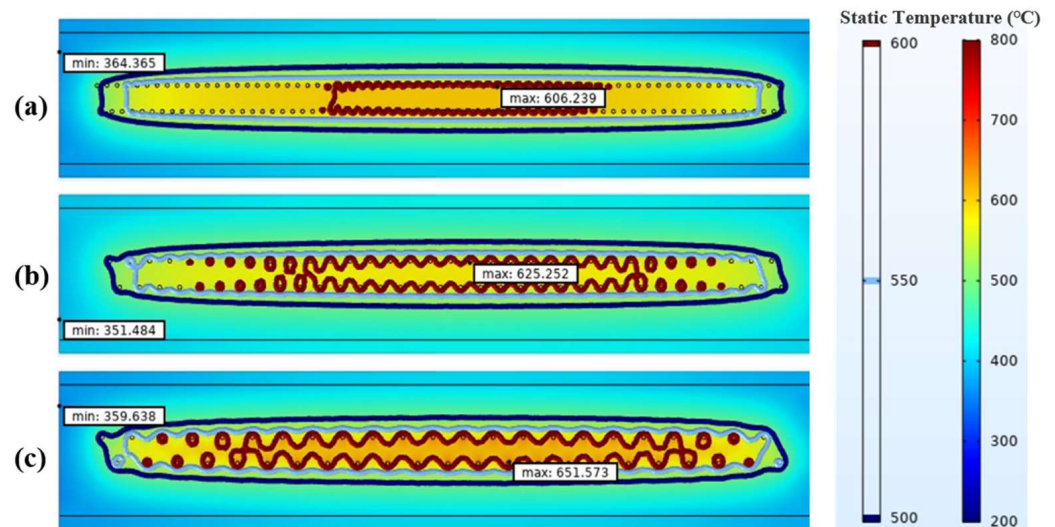
Figure 12. Temperature distribution isotherm diagram: (**a**) ES-P-01, (**b**) ES-P-02, and (**c**) ES-P-03.

Figure 13 compares the impact of the number of spiral wires on the temperature distribution of the foam electric heating catalyst. As the number of wires increases, the temperature difference between the highest and lowest points expands, measuring 174.1 °C, 209.2 °C, and 152.5 °C. When there are four wires, the temperature difference between the highest and lowest points inside the reactor is the smallest. Given the internal dimensions of the reactor, a configuration with four wires results in the most uniform temperature distribution. Moreover, it is noticeable in the diagram that more than 80% of the internal region attains a temperature of 640 °C, and by enhancing external insulation, the internal temperature of the catalyst can be made substantially uniform.
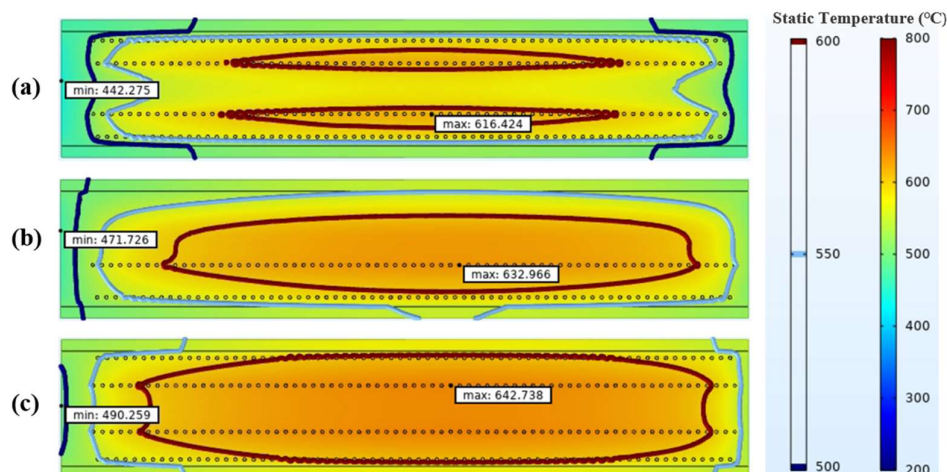
Figure 13. Temperature distribution isotherms: (**a**) ES-N-01, (**b**) ES-N-02, and (**c**) ES-N-03.

Taking into account the temperature distribution and heating wire processing complexity, the preferred configuration is a spiral heating wire with a diameter of 1 mm, a spiral diameter of 5 mm, a spiral pitch of 2, and a total of four spiral wires.

3.3. Internal Temperature Distribution Test and Comparative Analysis of the Reactor

To address these challenges in industrial applications, a reaction tube of similar industrial dimensions was designed. In this study, both electric heating catalysts and granular catalysts were analyzed and compared. The internal test structure is depicted in Figure 2b.

Investigating Figure 14, at 650 °C, 3000 h^{-1} and S/C = 3, utilizing an identical catalyst composition, the methane conversion of the ES-in demonstrates an approximate 9% increase in comparison to GC-out. Moreover, the hydrogen concentration exhibits a notable augmentation of 3.2%. Additionally, for the identical catalyst composition, variations in heat sources yield discernible discrepancies in catalytic performance. Relative to ES-out, EC-in results in an approximate 3% increase in methane conversion efficiency and a 2.1% increase in hydrogen concentration.
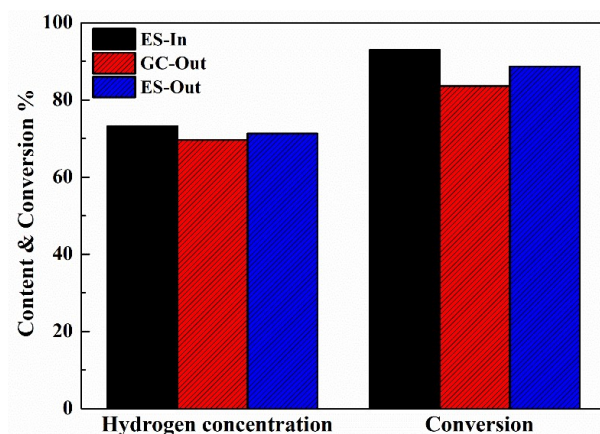

Figure 14. Catalyst performance comparison.

In the case of external heating, there is a significant radial temperature difference in the reaction tube. When the flow distribution in the tube is uneven, the temperature difference becomes greater. Ensuring temperature uniformity is crucial for improving methane conversion rates. When convective heat transfer from the heat source to the reforming zone is improved, the methane conversion rate is also positively affected. Additionally, the foam structure induces turbulence in the tube, enhancing the convective heat transfer coefficient in the tube, resulting in increased methane conversion rates.

In the presence of 650 °C, 3000 h^{-1}, and S/C = 3, the axial temperature and concentration variations within the reactor, as depicted in Figure 15. Figure 15a illustrates a significant temperature decrease at a distance of 10 cm in the anterior section of the reactor. Subsequently, there is another decrease at 30 cm. Conversely, in Figure 15c, the most substantial temperature drop occurs closer to the inlet, followed by a gradual increase, eventually surpassing the stable temperature prior to the reaction.
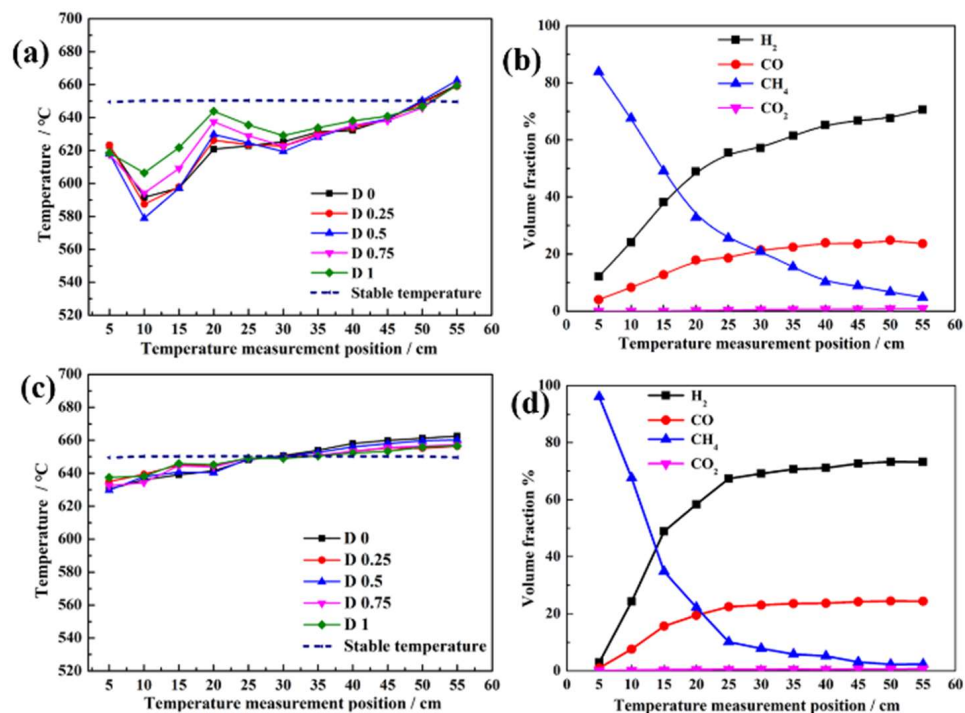
Figure 15. Axial temperature and concentration difference inside the reactor: (**a**) axial temperature difference of GC-out; (**b**) axial concentration difference of GC-out; (**c**) axial temperature difference of ES-in; (**d**) axial concentration difference of ES-in.

Evidently, the use of internal heating significantly ameliorates the overall axial temperature differences, owing to the internal-to-external heat transfer and the exceptional thermal response of the electrical heating filament, in comparison to external heating. The stable temperature decrease within the reactor is less than 40 °C with internal heating, representing a 69.4% reduction compared to external heating.

Figure 15b demonstrates that the majority of CH$_4$ conversion occurs in the proximity of the inlet (5–15 cm). Within the range of 15–30 cm, the concentrations of methane and hydrogen remain relatively stable. Similarly, within the 35–55 cm range, the concentrations of methane and hydrogen remain stable, exhibiting no significant variations. Along the axial direction, the methane steam reforming reaction rate rapidly diminishes downstream, contributing less to the total CH$_4$ conversion. A comparison between Figure 15b,d reveals that, although CH$_4$ concentration exhibits a similar declining trend, electrical heating leads to a faster decline. This can be attributed to the highly efficient internal heat transfer facilitated by electrical heating, effectively addressing issues such as inadequate preheating of methane and water, transient isothermal segments within the furnace, and insufficient internal heat transfer. Internal electrical heating significantly reduces the axial temperature differences within the entire reactor, resulting in a more uniform internal temperature distribution.

Figure 16 illustrates the temperature variation within the reactor during isothermal reactions of GC-out and ES-in at 650 °C, S/C = 3, and a space velocity of 5000 h^{-1}. In Figure 16a, two distinct temperature reduction peaks are observed at 10 cm and 30 cm. At 10 cm, the temperature instantaneously drops due to the strong endothermic reaction, and

the insufficient external heat transfer fails to rapidly restore the temperature, resulting in a subsequent temperature decrease at 15 cm and 20 cm, falling below the required reaction temperature and leading to reduced conversion rates. At 30 cm, the temperature is not immediately affected by the rapid temperature drop at 10 cm, allowing the reaction to proceed. However, inadequate heat transfer still causes a rapid temperature decrease at this point. In Figure 16b, compared to the GC-out, the temperature reduction with ES-in is lower. It is evident that the reaction zone of electric heating shifts notably forward, attributed to the fact that the temperature at the reactor inlet is not influenced by dissipation, resulting in lower temperatures. Two distinct temperature reduction peaks are also observed in this curve, at the inlet and 20 cm, but with significantly reduced peak heights, benefiting from the rapid temperature response of internal electric heating.
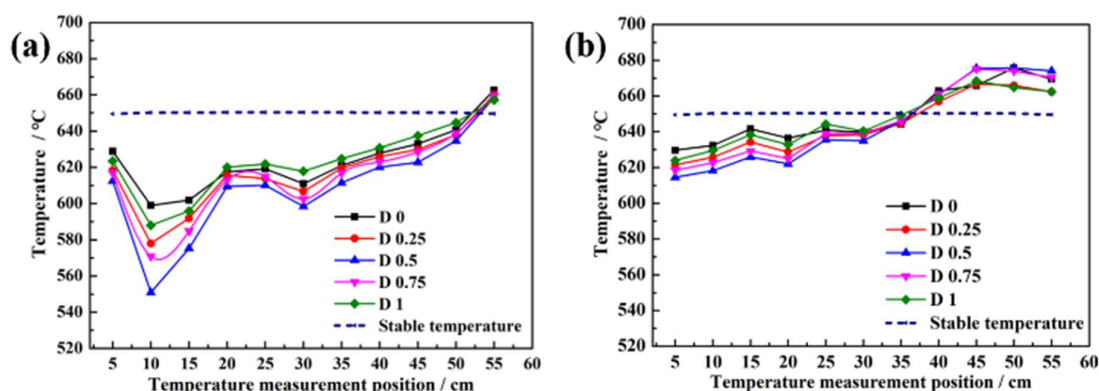

Figure 16. Comparison of axial temperature difference at 5000 h^{-1}: (**a**) GC-out; (**b**) ES-in.

For the ES-in, there is no noticeable cold spot due to the even distribution of high heat flux generated by internal heating. The good mass transfer of the electric heating wire and the catalyst coating quickly activates the reaction.

Figure 17a illustrates the temperature differences at 650 °C, S/C = 3, and 3000 h^{-1}. It is evident that the highest temperature decrease occurs at the inlet, followed by a gradual increase, consistent with the trend observed in ES-in. Figure 17b displays the temperature differences at 650 °C, S/C = 3, and 5000 h^{-1}. Unlike the conditions at 3000 h^{-1}, two distinct strong temperature reduction peaks are observed at the inlet and at 15 cm, resulting in a stable temperature decrease of 80 °C. It can be inferred that EC-out and GC-out exhibit similar reaction patterns, characterized by distinct temperature reduction peaks. With an increase in the reaction GHSV, these decrease peaks transition into multiple peaks. Consequently, the differences in temperature decrease between internal and external electrical heating are not primarily due to changes in internal materials, but rather stem from differences in heating methods.
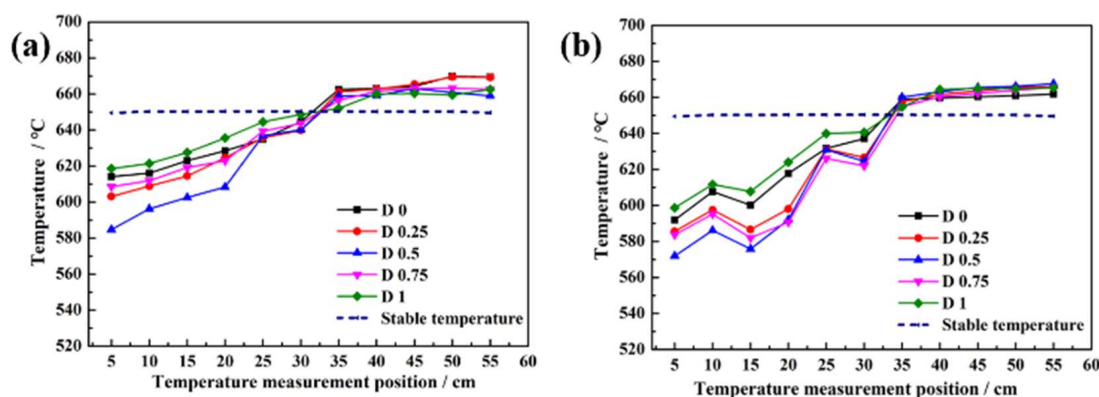

Figure 17. Axial temperature difference of ES-out: (**a**) 3000 h^{-1}; (**b**) 5000 h^{-1}.

At 650 °C, S/C = 3, and 3000 h^{-1}, the radial temperature differences are depicted in Figure 18. As shown in Figure 18a, it is evident that the radial temperature differences with external heating are significantly higher compared to electrical heating. External electric heating transfers heat from the outer wall of the reaction tube to the inside. Due to the limited heat transfer efficiency of the granular catalyst, the center temperature of the reactor is originally lower. Additionally, the endothermic reaction exacerbates the temperature drop, and this cannot be effectively compensated, resulting in a temperature difference of up to 60 °C between positions D0 and D0.5 in the reactor.
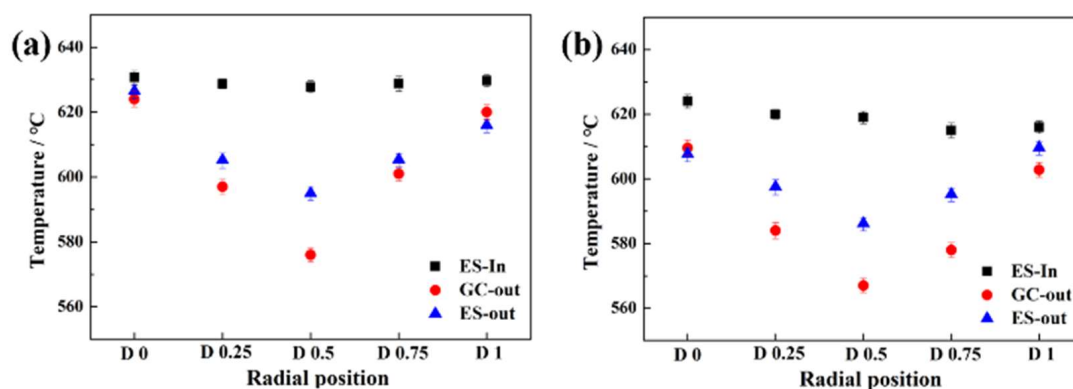

Figure 18. Radial temperature differences of reactor: (**a**) 3000 h^{-1}; (**b**) 5000 h^{-1}.

In contrast, the rapid response of the electric heating wire allows for quick compensation of temperature reduction in the electric heating catalyst. Furthermore, the electric heating wire inside has no heat transfer limitations, resulting in a much smaller radial temperature difference during the reaction, about 3 °C, which is 95% lower than that of external heating, leading to overall temperature uniformity. Even at 5000 h^{-1}, as shown in Figure 18b, the radial temperature difference with electrical heating is only 9 °C, which is significantly lower compared to external heating.

As depicted in Figure 19a, it is evident that ES-in exhibits a notably swifter temperature elevation compared to GC-out. Within a sizable reaction apparatus, the electric heating method achieves a temperature of 650 °C in a mere 23 min, signifying a 69% acceleration in comparison to the 76 min necessary for GC-out (with a maximum heating rate of 10 °C/min). Similarly, for external heating, ES-out (foam catalyst), due to its homogeneous internal structure without the presence of internal thermal resistance, exhibits a faster heating rate compared to GC-out. The porous and interconnected nature of the foam enhances heat transfer efficiency, leading to an accelerated temperature rise.
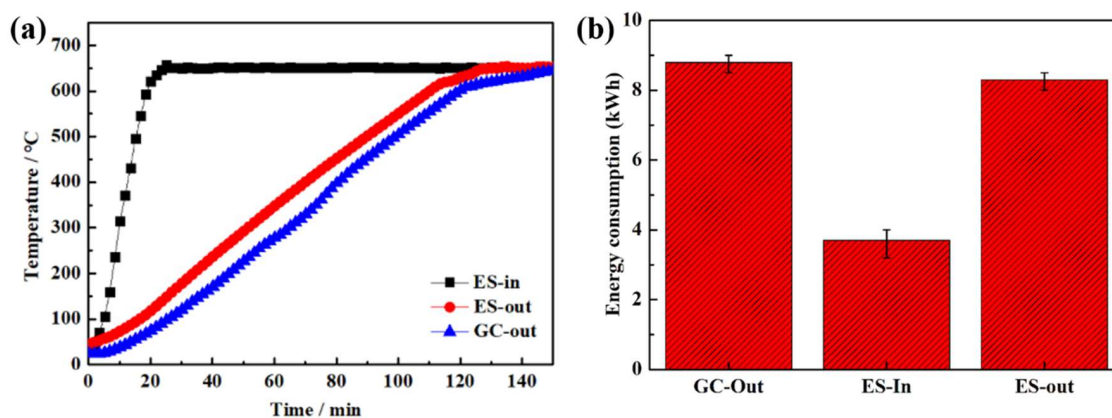

Figure 19. Temperature response and energy consumption. (**a**) Comparison of heating rate; (**b**) comparison of energy consumption.

Effective heat management is crucial for achieving optimal methane conversion rates, and heat transfer plays a significant role in this process [26]. Utilizing a highly conductive catalytic foam catalyst creates strong turbulent flux in the gas feed, improving heat and mass transfer, which in turn equalizes axial temperatures, enhances catalytic activity, and minimizes hot spots [27]. Choosing a substrate with high thermal conductivity further enhances hydrogen production efficiency and reduces costs [28].

At 650 °C, S/C = 3, 3000 h^{-1}, and a stable operation for 8 h, the energy consumption results of the corresponding reaction stage are illustrated in Figure 19b. It can be observed that, under the same reaction conditions and duration, the energy consumption of GC-out and ES-out does not differ significantly. However, the overall energy consumption of the electrically heated reactor is noticeably reduced, being 56.82% lower compared to external heating.

3.4. Discussion of Results

As shown in Figure 20, the electric heating wire, the foam substrate, and the catalyst coating are closely combined. When the electric heating wire is energized, the electric heating wire produces a rapid heat transfer to the adjacent catalyst coating, so that it heats up rapidly, which will improve the temperature response and heating characteristics of the catalyst. The catalyst in the form of foam can also increase the residence time of the reactants and improve the catalytic efficiency.
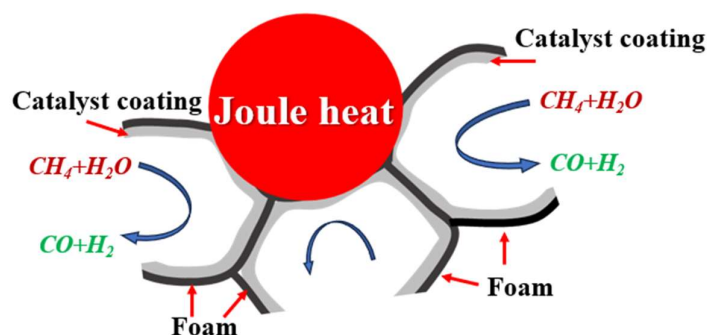

Figure 20. Internal reaction mechanism of the electrothermal catalyst.

The evenness of temperature within the reactor can be effectively adjusted by controlling the distribution of the electric heating wire. The highest temperature is concentrated within the catalyst, rather than on the reactor wall. Importantly, the amount of coating can be increased as needed, and the preparation process is less challenging compared to using metal foam and metal tubes. This results in a simpler, more compact reaction vessel that is easier to maintain. It also eliminates restrictions related to reaction tubes and coatings and simplifies insulation and amplification.

As depicted in Figure 21b, due to inherent transfer limitations, including catalyst particle constraints, reactor wall resistance, and flow impediments [12,29], external heating has a significant temperature gradient persists within the reactor. To elevate the temperature of the internal catalyst, it is imperative to augment the external combustion temperature, which, in turn, escalates energy expenditure. Concurrently, this strategy engenders an increase in internal carbon deposition. In contrast to the external combustion of natural gas, the electric heating catalyst exhibits superior thermal efficiency, thereby facilitating a more environmentally benign and low-carbon energy conversion process. The temperature of the electric heating catalyst is transferred from the inside to the outside, so that the internal temperature gradient can be reduced. Compared with the external combustion of natural gas, electric heating catalyst has higher thermal efficiency, resulting in green and low carbon.
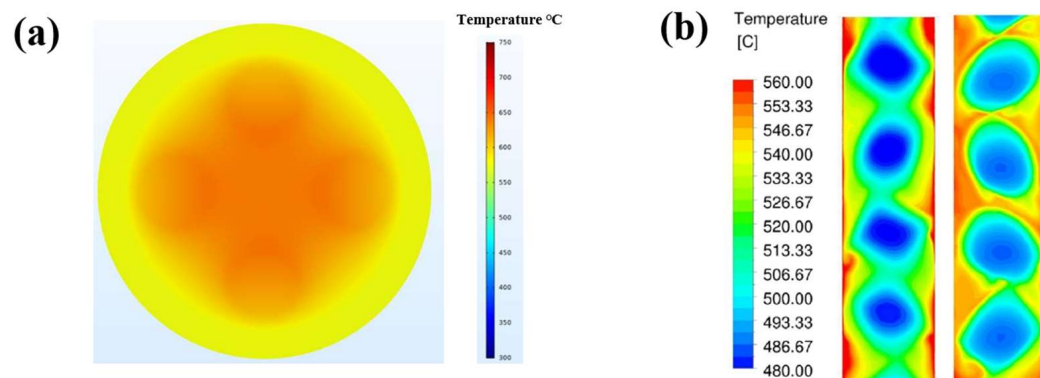
Figure 21. Internal temperature difference diagram of electric heating and conventional heating: (**a**) X-Z axis middle section of ES-N-03 and (**b**) external heating [29].

The existing industrial system's reactor, constructed from metallic materials, boasts superior mechanical strength, thermal conductivity, and pressure tolerance. However, the prevalent internal electric heating configurations, which predominantly employ conductive matrices, present formidable challenges in terms of insulation. In contrast, the ceramic foam structure proposed herein, diverging from conventional electric heating methodologies, obviates the necessity for specific material layers in the reactor. This approach significantly diminishes the application costs, as ceramics are economically more viable than traditional metallic materials. The ceramic material, fabricated via the replication template method, offers greater flexibility in altering the matrix dimensions, thereby enhancing its adaptability. The arrangement of electric heating wires can be tailored more precisely to specific demands, endowing this method with distinct advantages for industrial-scale applications. Therefore, this technology has broad application prospects in assisting industrial decarbonization.

However, there are still problems of high-voltage sealing and high-humidity insulation in practical applications, which still need further study. In future research, it is essential to delve into the stability of high-pressure reactions, sealing integrity, high-temperature stability, and the service life of reactors, further analyzing the systemic reliability risks posed by the contradictions between electrified experiments and hydrogen energy safety. Additionally, a cost analysis should be conducted on an equivalent scale to further optimize the prospects for industrial applications.

4. Conclusions

In this work, we introduced an electrically heated structural catalyst. This catalyst, along with the associated electric heating wire and foam catalyst, was fabricated using a one-step method. Notably, the catalyst is characterized by a high coating amount and ease of scale-up. The configuration of the electric heating wire was refined through simulation techniques, allowing us to preliminarily establish optimal preparation parameters. Subsequently, utilizing a self-constructed experimental test platform and an electric heating reaction tube, we systematically compared the axial and radial temperature variance, as well as the performance of methane steam reforming for hydrogen production, energy efficiency, and other relevant aspects against the conventional external heating method. The principal findings are summarized as follows:

(1) Electric heating only required 25 min to reach 650 °C, saving 64% of the time compared to external electric heating; electric heating demonstrates a highly stable temperature distribution, with minimal variations in reactor temperature within a GHSV range of 500–10,000 h^{-1}.

(2) A Ni/Al_2O_3/ceramic foam Joule electric heating catalyst was developed, and wire distribution was simulated. The best temperature distribution inside the reactor was achieved when using a spiral wire with a final diameter of 1 mm, a spiral diameter of 5 mm, a spiral pitch of 2, and a total of four spiral wires.

(3) At 650 °C, S/C = 3, and 3000 h^{-1}, compared to external heating, internal electrical heating can achieve a reduction of 69.4% in the axial temperature differences within the reactor, while achieving a 95% reduction in the radial temperature differences.

(4) Internal-to-external heat supply and close proximity between electric heating and foam catalyst make the electric heating catalyst reach 72% energy efficiency at 650 °C.

The scheme proposed in this paper offers advantages in insulation, cost, amplification effects, and energy efficiency. Moreover, there is considerable scope for optimization in terms of wire distribution, foam structure, and dimensions. It is hoped that this provides a referenceable approach for the electrification applications in the hydrogen production industry.

Author Contributions: Y.R.: Conceptualization, Methodology, and Writing—original draft. L.Z.: Writing—review and editing. H.X.: Investigation, Data curation, and Supervision. All authors have read and agreed to the published version of the manuscript.

Conflicts of Interest: The authors declare that they have no known competing financial interests or personal relationships that could have appeared to influence the work reported in this paper.

References

1. Kumar, R.; Singh, R.; Dutta, S. Review and Outlook of Hydrogen Production through Catalytic Processes. *Energ. Fuel.* **2024**, *38*, 2601–2629. [CrossRef]
2. Harrison, D. Sorption-enhanced hydrogen production: A review. *Ind. Eng. Chem. Res.* **2008**, *47*, 6486–6501. [CrossRef]
3. Wilhite, B.A.; Breziner, L.; Mettes, J.; Bossard, P. Radial microchannel reactors (RMRs) for efficient and compact steam reforming of methane: Experimental demonstration and design simulations. *Energ. Fuel.* **2013**, *27*, 4403–4410. [CrossRef]
4. Lee, J.S.; Seo, J.; Kim, H.Y.; Chung, J.; Yoon, S.S. Effects of geometry and operating conditions on hydrogen productivity of a fuel cell reformer. *Int. J. Heat. Mass. Transfer.* **2014**, *73*, 318–329. [CrossRef]
5. Ratnakar, R.R.; Balakotaiah, V. Modular reactors with electrical resistance heating for hydrocarbon cracking and other endothermic reactions. *AIChE J.* **2022**, *68*, e17542. [CrossRef]
6. Spagnolo, D.A.; Cornett, L.J.; Chuang, K.T. Direct electro-steam reforming: A novel catalytic approach. *Int. J. Hydrogen Energy* **1992**, *17*, 839–846. [CrossRef]
7. Holladay, J.D.; Hu, J.; King, D.L.; Wang, Y. An overview of hydrogen production technologies. *Catal. Today* **2009**, *139*, 244–260. [CrossRef]
8. Le Quéré, C.; Moriarty, R.; Andrew, R.M.; Canadell, J.G.; Sitch, S.; Korsbakken, J.I.; Friedlingstein, P.; Peters, G.P.; Andres, R.J.; Boden, T.A.; et al. Global carbon budget 2015. *Earth Syst. Sci. Data.* **2015**, *7*, 349–396. [CrossRef]
9. Dinh, D.; Trenchev, G.; Lee, D.; Bogaerts, A. Arc Plasma Reactor Modification for Enhancing Performance of Dry Reforming of Methane. *J. CO$_2$ Util.* **2020**, *42*, e101352. [CrossRef]
10. Wang, Q.; Wang, J.; Zhu, T.; Zhu, X.; Sun, B. Characteristics of methane wet reforming driven by microwave plasma in liquid phase for hydrogen production. *Int. J. Hydrogen Energy* **2021**, *46*, 34105–34115. [CrossRef]
11. Scarfiello, C.; Bellusci, M.; Pilloni, L.; Pietrogiacomi, D.; La Barbera, A.; Varsano, F. Supported Catalysts for Induction-Heated Steam Reforming of Methane. *Int. J. Hydrogen Energy* **2020**, *46*, 134–145. [CrossRef]
12. Wismann, S.T.; Engbæk, J.S.; Vendelbo, S.B.; Bendixen, F.B.; Winnie, L.; Aasberg-Petersen, K.; Frandsen, C.; Chorkendorff, I.; Mortensen, P.M. Electrified Methane Reforming: A Compact Approach to Greener Industrial Hydrogen Production. *Science* **2019**, *364*, 759756–759759. [CrossRef] [PubMed]
13. Wismann, S.T.; Engbæk, J.S.; Vendelbo, S.B.; Eriksen, W.L.; Frandsen, C.; Mortensen, P.M.; Chorkendorff, I. Electrified Methane Reforming: Understanding the Dynamic Interplay. *Ind. Eng. Chem. Res.* **2019**, *58*, 23380–23388. [CrossRef]
14. Rieks, M.; Bellinghausen, R.; Kockmann, N.; Mleczko, L. Experimental Study of Methane Dry Reforming in an Electrically Heated Reactor. *Int. J. Hydrogen Energy* **2015**, *40*, 15940–15951. [CrossRef]
15. Zheng, L.; Ambrosetti, M.; Marangoni, D.; Beretta, A.; Groppi, G.; Tronconi, E. Electrified methane steam reforming on a washcoated SiSiC foam for low-carbon hydrogen production. *AIChE J.* **2023**, *69*, e17620. [CrossRef]
16. Ambrosetti, M.; Beretta, A.; Groppi, G.; Tronconi, E. A numerical investigation of electrically-heated methane steam reforming over structured catalysts. *Front. Chem. Sci. Eng.* **2021**, *3*, e53. [CrossRef]
17. Badakhsh, A.; Kwak, Y.; Lee, Y.-J.; Jeong, H.; Kim, Y.; Sohn, H.; Nam, S.W.; Yoon, C.W.; Park, C.W.; Jo, Y.S. A compact catalytic foam reactor for decomposition of ammonia by the Joule-heating mechanism. *Chem. Eng. J.* **2021**, *426*, e130802. [CrossRef]

18. Dou, L.; Yan, C.; Zhong, L.; Zhang, D.; Zhang, J.; Li, X.; Xiao, L. Enhancing CO_2 Methanation over a Metal Foam Structured Catalyst by Electric Internal Heating. *Chem. Commun.* **2020**, *56*, 205–208. [CrossRef]

19. Zheng, L.; Ambrosetti, M.; Zaio, F.; Beretta, A.; Groppi, G.; Tronconi, E. Direct electrification of Rh/Al_2O_3 washcoated SiSiC foams for methane steam reforming: An experimental and modelling study. *Int. J. Hydrogen Energy* **2023**, *48*, 14681–14696. [CrossRef]

20. Shin, G.; Yun, J.; Yu, S. Thermal design of methane steam reformer with low-temperature non-reactive heat source for high efficiency engine-hybrid stationary fuel cell system. *Int. J. Hydrogen Energy* **2017**, *42*, 14697–14707. [CrossRef]

21. Ren, Y.; Xu, H.; Wang, Q.; Kuang, X.; Zhang, L.; Li, G. Preparation and performance analysis of integrated electric heating hydrogen production foam catalyst. *Int. J. Hydrogen Energy* **2024**, *56*, 699–708. [CrossRef]

22. Rahimipetroudi, I.; Shin, J.S.; Rashid, K.; Yang, J.B.; Dong, S.K. Development and CFD analysis for determining the optimal operating conditions of 250 kg/day hydrogen generation for an on-site hydrogen refueling station (HRS) using steam methane reforming. *Int. J. Hydrogen Energy* **2021**, *46*, 35057–35076. [CrossRef]

23. Meloni, E.; Martino, M.; Ricca, A.; Palma, V. Ultracompact methane steam reforming reactor based on microwaves susceptible structured catalysts for distributed hydrogen production. *Int. J. Hydrogen Energy* **2021**, *46*, 13729–13747. [CrossRef]

24. Wang, Q.; Ren, Y.; Liu, H.; Liu, H.; Wang, X.; Gu, Z.; Zhang, L. Simulation and enhancement of axial temperature distribution in a reactor filled with in-situ electrically heated structured catalyst. *Int. J. Hydrogen Energy* **2024**, *55*, 217–224. [CrossRef]

25. Zhuang, X.; Xu, X.; Li, L.; Deng, D. Numerical investigation of a multichannel reactor for syngas production by methanol steam reforming at various operating conditions. *Int. J. Hydrogen Energy* **2020**, *45*, 14790–14805. [CrossRef]

26. Jin, M.-H.; Lee, C.-B.; Lee, D.-W.; Lee, S.-W.; Park, J.-W.; Oh, D.; Hwang, K.-R.; Lee, K.-Y.; Park, J.-S. Microchannel methane steam reformers with improved heat transfer efficiency and their long-term stability. *Fuel* **2016**, *176*, 86–92. [CrossRef]

27. Palma, V.; Ruocco, C.; Castaldo, F.; Ricca, A.; Boettge, D. Ethanol steam reforming over bimetallic coated ceramic foams: Effect of reactor configuration and catalytic support. *Int. J. Hydrogen Energy* **2015**, *40*, 12650–12662. [CrossRef]

28. Ricca, A.; Palma, V.; Martino, M.; Meloni, E. Innovative catalyst design for methane steam reforming intensification. *Fuel* **2017**, *198*, 175–182. [CrossRef]

29. Pashchenko, D.; Eremin, A. Heat flow inside a catalyst particle for steam methane reforming: CFD-modeling and analytical solution. *Int. J. Heat. Mass. Tran.* **2021**, *165*, 120617–120625. [CrossRef]